Rethinking transport
27–30 April 2020

TRA 2020 HELSINKI

Proceedings of 8th Transport Research Arena TRA 2020, April 27-30, 2020, Helsinki, Finland

The H2020 project FITGEN: preliminary results and design guidelines of an integrated e-axle for the third-generation electric vehicles

Michele De Gennaro[a,1], Peter Scheuermann[a], Tobias Wellerdieck[b], Vittorio Ravello[c], Gianmario Pellegrino[d], Elena Trancho[e]

[a]*AIT Austrian Institute of Technology GmbH, Giefinggasse 4, Vienna, 1210, Austria*
[b]*BRUSA Elektronik AG, 9466 Sennwald, Switzerland*
[c]*Centro Ricerche FIAT SCpA, Strada Torino 50, 10043 Orbassano, Italy*
[d]*Department of Energy "Galileo Ferraris", Politecnico di Torino, Corso Duca degli Abruzzi 24, 10129, Torino, Italy*
[e] *TECNALIA, Parque Tecnológico de Bizkaia, E-48160 Derio, Bizkaia, Spain.*

Abstract

The electrification of light-duty vehicles is key to reducing emissions in urban areas. This paper aims at presenting the interim results of the European project FITGEN, granted under the H2020 LC-GV-01-2018 call and kicked-off in January 2019. The project will deliver an e-axle natively designed to fit a brand-independent A-segment fully electric vehicle architecture, enabling the following progresses beyond the state-of-the-art 2018: (1) 40% increase of power density of the motor from an innovative 6-phase permanent magnet e-machine design with operation at 20,000 rpm, (2) 50% increase of power density of the inverter from the adoption of SiC power switches and (3) affordable, in-built fast charge capability up to 120 kW peak power. This manuscript includes the design guidelines adopted in the areas of electric motor, transmission, power electronics and control, providing an interim overview of the advancements of the project.

Keywords: H2020 FITGEN, e-axle, third generation electric vehicles, electric motor, SiC inverter, fast charging.

[1] Corresponding author. Tel.: +43 50550 6249;
E-mail address: michele.degennaro@ait.ac.at; michele.degennaro.phd@gmail.com

List of main acronyms

2WD	2 Wheel Drive	IGBT	Insulated-Gate Bipolar Transistor
4WD	4 Wheel Drive	MOSFET	Metal-Oxide-Semiconductor Field-Effect Transistor
AC	Alternating Current		
BEV	Battery Electric Vehicle	NMC	Nickel Manganese Cobalt
BPM-SM	Buried-Permanent-Magnet Synchronous Machine	OEM	Original Equipment Manufacturer
		PHEV	Plug-in Hybrid Electric Vehicle
DC	Direct Current	PWM	Pulse-Width Modulation
CRF	Centro Ricerche Fiat	SOA	Safe Operating Area
FITGEN	Functionally Integrated E-axle Ready for Mass Market Third Generation Electric Vehicles	SiC	Silicon Carbide
		SUV	Sport Utility Vehicle
		TRL	Technology Readiness Level
FLW	Form Litz Wire	VA	Volt-Ampere
GaN	Gallium Nitride	WLTP	Worldwide harmonized Light vehicle Test Procedure
H2020	Horizon 2020		
HPW	Hairpin Winding	xEV	battery electric, plug-in hybrid and hybrid vehicles altogether
ICE	Internal Combustion Engine		

1. Introduction

Electrification is the macrotrend that has mostly influenced research and development activities in transport during the last decade. The European Union has significantly invested in low-carbon transport technologies under the H2020 programme, with more than 30 billion EUR of public funding invested in transport research and infrastructures in the period 2014-20. In the field of road transport, this decade has witnessed the phasing out of the research and development activities on combustion engines, with the shift of resources towards hybrid and electric vehicle technologies. The activities have been focused on advancing two key enabling technologies for electric vehicles: Li-ion batteries and electric powertrains.

The development path in the field of Li-ion batteries is indicated in the SET-plan Action 7 (EU Commission, 2016), which has seen the deployment of the Generation 2b batteries (Ni-based NMC 523 and 622) in the first half of the decade, to shift towards a progressive reduction of cobalt in the Generation 3a (NMC 811) in 2020, and towards further reduction or elimination of critical raw materials while increasing energy density (high energy NCM and high voltage spinel, Generation 3b) by 2025, before transitioning to solid state electrolytes (Generation 4). In the field of electric powertrains, development mostly focuses on the delivery of next generation electric motors and next generation power converters. In the first case, the trend moves in the direction of increasing the power density and the rotational speed of the electric motor (above 5 kW/kg peak power and 20,000 rpm), while in the second case, the trend consists in replacing IGBT MOSFETs with high-frequency power switches based on SiC and GaN technologies, allowing for higher switching speeds and thus higher power densities while increasing efficiency of the power inverter (25 kW/litre and 98-99% peak efficiency on the homologation cycle). The development trend also pushes towards the reduction of the production costs. According to (Boston Consulting , 2018) BEVs are up to 35% more expensive than ICE vehicles in 2018. While on average the cost of an ICE vehicle is split in 16% for the powertrain and 84% for other parts, BEV cost is composed of 15% for the powertrain, 35% for the battery pack and 50% for other parts. Therefore, on one side, the cost of the battery needs to be halved compared to actual figures (target values indicate 90 €/kWh for 2025-30 production at pack level), while on the other side, powertrain costs need to be reduced by one third, to shave the cost premium of electric vehicles against conventional fuel vehicles. Both economies of scale and new technologies and materials will contribute to cost reductions. Concerning the first, new registrations of electric cars accounted for 1.23 million units worldwide in 2017, with 1.07 million additional units sold January to September 2018 (Insideevs.com, 2018). More than 4 million electric vehicles were circulating worldwide by December 2018, with a 30% share in Europe. China and the US, in turn, each cover approximately 30 % of the global fleet, with Japan making up for the remaining 10% (IEA, 2018). Recent figures suggest an xEV market share of 6% by 2020, 24% by 2025 and 48% by 2030 (Boston Consulting , 2018). Approximately 24 million vehicles per year are expected to be sold by 2030, for a global market turnover above 700 billion € per year, of which 50 billion € on electrified powertrains. Concerning new technologies and materials, the adoption of (i) SiC-based inverter, (ii) copper-dense stator winding (e.g. formed litz wire, as later discussed in section 3), (iii) rare-earth scarce high-coercivity magnets and (iv) advanced design and production techniques will enable a better integration of the powertrain components, thus improving

performance and decreasing costs. In this context, the H2020 project FITGEN (Functionally Integrated E-axle Ready for Mass Market Third Generation Electric Vehicles) has been granted under the call LC-GV-01-2018 (EU Commission CORDIS, 2019). The project consortium consists of the research center from the reference automotive OEM (CRF) combined with suppliers in the field of motor/inverter (BRUSA), SiC power devices (ST-Microelectronics) and transmission (GKN), supported by two research partners (AIT and Tecnalia) and two Universities (Politecnico of Torino and University of Brussels). The project has an overall budget of 5.8 million € and a funding of 5.0 million € and it aims at developing a functionally integrated e-axle ready for implementation in the third-generation electric vehicles (i.e. 2025 and beyond). The e-axle is made by of a 6-phase Buried-Permanent-Magnet Synchronous Machine (BPM-SM), driven by a SiC-inverter and coupled with a single speed transmission. It is complemented by a DC/DC-converter for high voltage operation of the motor in traction and for enabling fast charging of the battery (120 kW-peak) plus an integrated AC/DC on-board charger. Figure 1 reports a schematic of the architecture of the FITGEN e-axle, with its different components and a simplified electrical scheme.

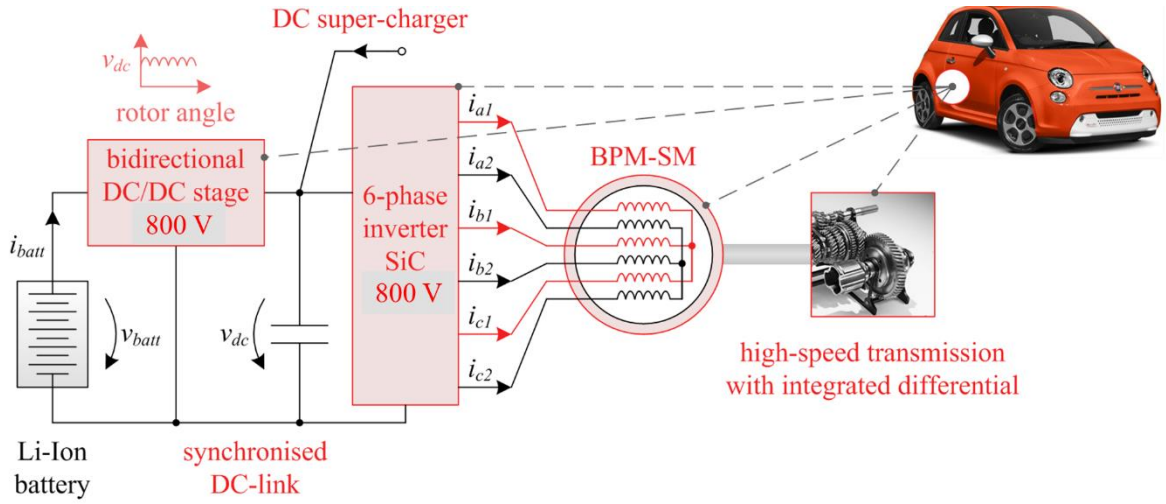

Figure 1: FITGEN e-axle overall architecture (reported graphics are indicative; the final implementation of the e-axle might change).

The e-axle aims at achieving the following advances beyond the SotA 2018:

- 40 % increase of the power density of the BPM-SM, i.e. 5.0 kW/kg with operation at 20,000 rpm and peak efficiency at 96.5%;
- 50 % increase of the power density of the SiC-inverter, 25 kW/l and peak efficiency at 98-99%;
- affordable and integrated fast charge capability (80 kW, average);
- production cost target at 2,000 €/unit (2030 market, cost of BPM-SM, power electronics and transmission);

The e-axle is delivered at the end of the project at TRL 7 (i.e. system prototype demonstration in operational environment), in all its components and demonstrated on an electric vehicle platform designed for the European market (A-segment reference platform, i.e. FIAT 500-electric, as per Figure 1). The project has been kicked-off in January 2019 and it runs for 36 months, i.e. up until December 2021. At present, it is still in an initial phase with few results ready to be presented. In this regard, this paper aims at presenting the overall concept of FITGEN, the earliest results concerning reference vehicle platforms and end-user requirements adopted, the earliest results concerning e-axle integration within the demonstrator and the guidelines that will be adopted for the design of the BPM-SM, single-speed transmission, SiC-inverter, DC/DC converter and integrated on-board charger.

2. Reference vehicle platforms, end-user requirements and sizing of the FITGEN e-axle

The FITGEN e-axle is natively designed to be implemented and demonstrated on a A-segment BEV platform; however, to exploit at full its potential, it must also accomplish multi-brand and multi-platform applications. To this purpose, three vehicle platforms have been considered for its preliminary sizing: (1) the A-segment BEV in 2WD configuration planned for its demonstration, (2) a small SUV in PHEV 4WD configuration with the combustion engine on the front axle and the electric traction on the rear axle, and (3) a large SUV BEV in 4WD configuration with the electric traction on both front and rear axle. Table 1 reports the main design parameters and target performance identified for the three reference platforms; note that the target performance for the small SUV

is calculated in EV mode only (i.e. charge depleting mode), and that the maximum road slope from standstill is estimated under an acceleration of 0.05 g with 10 km/h maximum speed. A set of speed profiles, including both type approval (WLTP and US06) and real driving cycles (urban and mixed, both acquired in Torino, Italy), have been considered to size the e-axle. Additionally, a highway driving cycle at 110 km/h constant speed has been considered, with a target electric driving range above 700 km with one fully charged battery at the beginning plus three stops for fast charging in-between. Based on these end-user requirements, the electric motor has been sized considering two reduction ratios for the single speed transmission, i.e. 1:9.6 and 1:12.5. The most demanding condition has been found for both reduction ratios for the Large SUV platform, at a maximum torque of 240 Nm and corner speed of 3,800 rpm for the 1:9.6 ratio and at a maximum torque of 180 Nm and corner speed of 4,800 rpm for the 1:12.5 ratio.

Table 1: Vehicle parameters and target performance.

Parameters	*Unit*	*A-segment*	*Small SUV*	*Large SUV*
Tyre rolling radius	m	0.3	0.32	0.34
Vehicle mass	kg	1,400	1,700	2,400
Rolling resistance	-	0.007	0.008	0.008
Product of drag coefficient and front area	m^2	0.75	0.9	0.85
Average 12V auxiliaries power	W	300	500	700
Target performance				
Maximum speed	km/h	160	130	220
Acceleration time 0-100 km/h	s	10	12	7
Maximum road slope from standstill	%	30	30	45
High speed grade @ 100 km/h	%	5	5	5

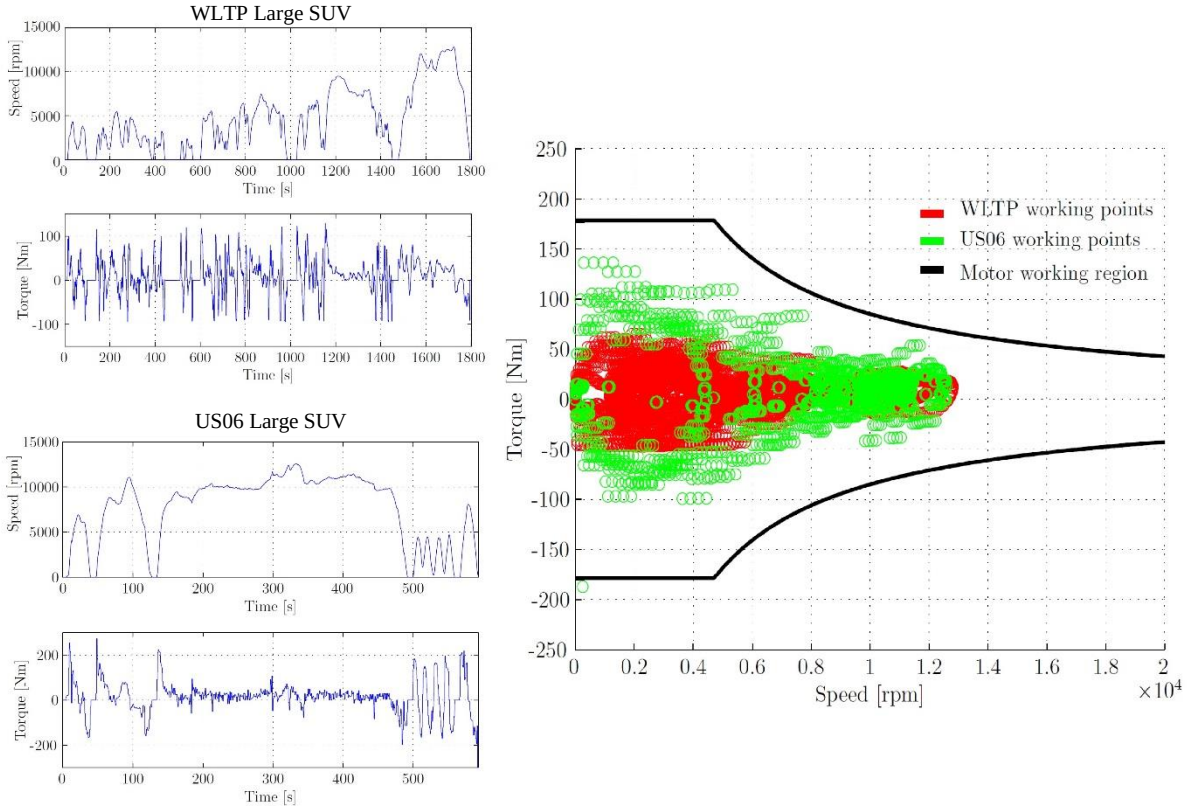

Figure 2: FITGEN electric motor torque vs. rpm envelope and WLTP/US06 operational points for the large SUV vehicle platform with reduction ratio of 1:12.5.

The FITGEN preliminary design choice favours the 1:12.5 solution, because it allows for operating the electric motor in a range between 20,000 and 22,000 rpm. In fact, higher rotational speed allows for higher power density of the electric motor. As an example, Figure 2 reports the torque vs. rpm envelope for the large SUV vehicle

platform with a reduction ratio of 1:12.5 (design condition), showing the operational points for the reference WLTP and US06 homologation cycles. Additionally, a virtual integration study of the e-axle with the project demonstrator A-segment vehicle platform has been carried out. This activity has considered 5 different integration architectures (including both front and rear axle), comparatively assessing complexity, integration level, feasibility of the project targets and mechanical interference of the e-axle with other components and systems. The selected integration architecture is depicted in Figure 3; the group inverter-motor-transmission is integrated as a mono-block (left), on top of which the DC/DC is installed (center), minimising the cable length. The e-axle is then mounted in rear wheel driving configuration (right) in the vehicle prototype chassis, using the space in the trunk and applying a mechanical modification to the rear suspension system to fit the new components.

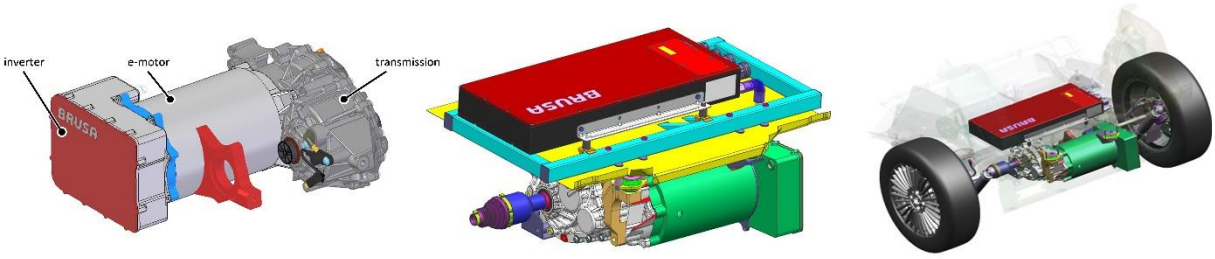

Figure 3: FITGEN inverter-motor-transmission group (left), integration of this group with the DC/DC converter (center) and integration of the full e-axle with the project validator A segment vehicle prototype rear axle (right).

3. The FITGEN e-axle components and design guidelines

3.1. Design guidelines for the Buried-Permanent-Magnet Synchronous Machine

The preliminary design considerations for the BPM-SM of the e-axle concern the choices of the target rotational speed and winding technology to achieve the requirements in Table 1. The choice of the target rotational speed must be made together with an evaluation of the geometrical properties of the machine, of the cooling requirements, and of the losses. This is illustrated with the use of a general scaling law for electric machines in traction applications. Furthermore, two candidates for the winding technology are considered: Hairpin Winding (HPW) and Form Litz Wire (FLW). It is shown how FLW allows for a better exploitation of the scaling law, enabling a higher power density.

3.1.1. Scaling law for the electric traction motor and evaluation of its performance

The scaling law for the electric traction motor assumes that the geometry of the BPM-SM, c.f. Figure 4, is scaled congruently, i.e. the ratio of the machine length and the radius is constant. Furthermore, the number of phases m, the number of magnetic pole-pairs n_p, the winding number N_w, etc. are constant. The tangential speed of the rotor v_T is assumed constant to ensure that the mechanical strength of the rotor material is fully utilized. The mechanical angular speed ω_m, the electrical angular speed ω_e and the electric frequency f_e are

$$\omega_m = v_t / r_{rotor}\,,\ f_e = \omega_m,\ f_e = \omega_e / 2\pi \propto r^{-1} \tag{1}$$

with the rotor radius r_{rotor} being linearly dependent on the machine radius r.

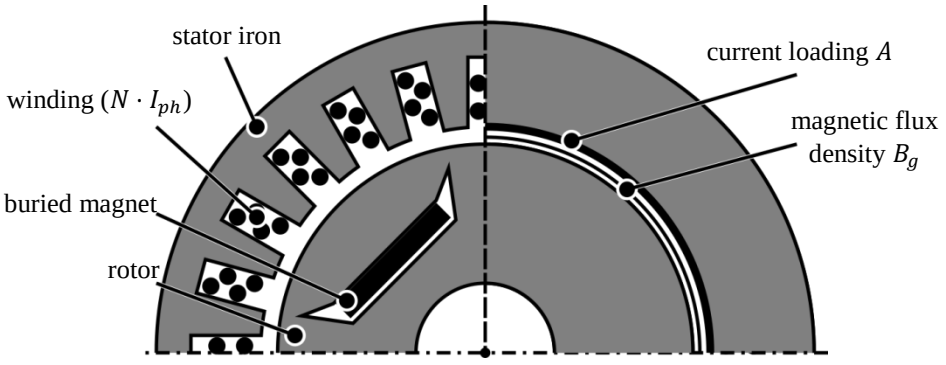

Figure 4: Schematic view of the BPM-SM and the simplification with current loading and flux density in the air gap.

The cooling thermal aspects are also considered by assuming that the machine and the stator temperature, ϑ_m and ϑ_c, as well as the heat transfer coefficient c_c are constant. Based on these assumptions, the cooling capability becomes

$$P_c = c_c A_c(\vartheta_m - \vartheta_c) \propto r^2 \tag{2}$$

with A_c being the cooling surface of the machine. The proportionality results from (1). The combination of a constant stator temperature and (2) leads to a scaling constraint for the iron and the copper losses, P_{fe} and P_{cu}, proportional to r^2. The Steinmetz formula to approximate the iron losses is

$$P_{fe} = c_{fe} f_e^{\alpha} B_{fe}^{\beta} \rho_{fe} V_{fe} \tag{3}$$

with $c_{fe}, \alpha, \beta, B_{fe}, \rho_{fe}$ and V_{fe} denoting the Steinmetz coefficients, the magnetic flux density in the iron and the density as well as the volume of the iron, respectively. Equation (2) and (3) and assuming that the flux density in the iron is proportional to the flux density in the air gap B_g leads to

$$P_{fe} \propto f_e^{\alpha} B_g^{\beta} r^3 \Rightarrow B_g \propto r^{\frac{\alpha-1}{\beta}} \tag{4}$$

A similar approach is usable for the copper losses P_{cu}, depending on the phase resistance R_{ph} and the current loading A according to

$$P_{cu} \propto I_{ph}^2 R_{ph} \qquad A = N_w I_{ph}/\tau_p \propto I_{ph}/r \qquad R_{ph} \propto N_w l_w / A_w \propto r^{-1} \tag{5}$$

with I_{ph}, l_w and A_w denoting the phase current, the length and the cross section of the winding, respectively. Using the proportionality of P_{cu} to r^2 and (5) leads to the scaling relation

$$A^2 r \propto r^2 \Rightarrow A \propto r^{\frac{1}{2}} \tag{6}$$

The torque produced by the machine is

$$T \approx \sigma \cdot (2\pi\, r_{rotor} l_{act}) \cdot r_{rotor} \propto \sigma r^3 \tag{7}$$

with r_{rotor}, l_{act} and σ denoting the rotor radius, the active length and the force density in the air gap, respectively. The force density in the air gap is

$$\sigma \propto A B_g \propto r^{\left(\frac{1}{2}+\frac{\alpha-1}{\beta}\right)} \Rightarrow T \propto r^{\left(\frac{7}{2}+\frac{\alpha-1}{\beta}\right)} \tag{8}$$

using (5) and (6). The power of the machine is

$$P = T\omega_m \propto r^{\left(\frac{7}{2}+\frac{\alpha-1}{\beta}\right)} \cdot r^{-1} = r^{\left(\frac{5}{2}+\frac{\alpha-1}{\beta}\right)} \tag{9}$$

and the power density is

$$P/V \propto r^{\left(\frac{5}{2}+\frac{\alpha-1}{\beta}\right)} \cdot r^{-3} = r^{\left(-\frac{1}{2}+\frac{\alpha-1}{\beta}\right)} \tag{10}$$

This shows that the power density of the machine can be improved by increasing the speed if

$$(\alpha - 1)/\beta < 1/2 \tag{11}$$

which is valid for laminated electric steel at frequencies where hysteresis losses are relevant. Similarly, the copper losses in (5) are only valid for frequencies at which skin and proximity effects in the winding are not significant. These two effects impose a lower limit for the size to which (10) is applicable. Furthermore, (4) is only valid until saturation in the iron becomes significant, otherwise B_g can no longer be increased, imposing an upper sizing limit to (10). Therefore, changing r by a large extent, e.g. by more than one order of magnitude, requires a more thorough analysis (Borisavljevic, 2013). Finally, it must be stated that (3) is only a valid approximation for magnetic fields with small harmonic distortion. However, a similar derivation for B_g is possible with the improved generalized Steinmetz equation (Mühlethaler, Biela, & Kolar, 2012).

3.1.2. Winding technology analysis

The scaling considerations in section 3.1.1 assume that the frequency dependency of the copper losses is negligible. A better approximation for the copper losses is

$$P_{Cu} \propto I_{ph}^2 R_{ph,AC}(f_e) \tag{12}$$

with the frequency dependent AC-phase resistance $R_{ph,AC}$. Two types of winding technology are analyzed: HPW and FLW. HPW is shown in Figure 5-a, with the rectangular solid copper conductor. This solution allows for a good slot fill factor it also leads to significant AC losses due to skin and proximity effects (Boldea & Nasar, 2010). FLW, instead, consists of stranded conductors that are inserted into the stator slots. An example is shown in Figure 5-b with two form litz bars inserted into each stator slot. FLW exhibits a slot fill factor that is worse than HPW, but the skin and proximity effects are greatly reduced. In the following $R_{ph,AC}$ is normalized to the DC-phase resistance $R_{ph,DC}$ to ensure a fair comparison between HPW and FLW, the normalization ratio is

$$k_f = \frac{R_{ph,AC}(f_e)}{R_{ph,DC}} \tag{13}$$

The normalization rate is calculated for

$$f \in [0, f_{max}] \tag{14}$$

with the maximum frequency f_{max} depending on the number of pole-pairs and the maximum motor speed. The frequency dependency of k_f for HPW and FLW can be calculated according to (Boldea & Nasar, 2010) and (Sullivan & Zhang, 2014). Since in FITGEN a mechanical speed of the BPM-SM at 20,000 rpm is required, this leads to high electric frequencies, thus making the use of FLW necessary to achieve superior performance.

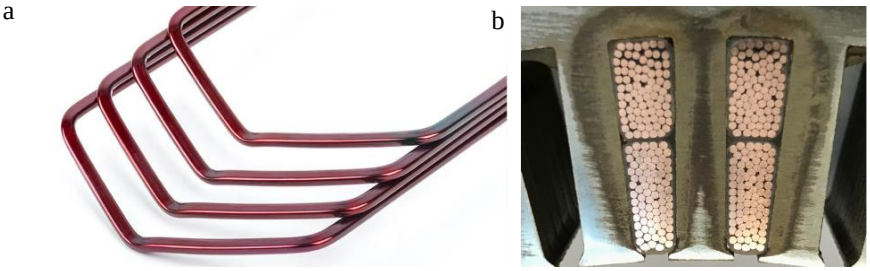

Figure 5: (a) hairpins for HPW (image courtesy of ATOP), (b) cross-section of FLW in the stator (BRUSA proprietary motor).

3.2. Design guidelines for the single-speed transmission

The electric motor and the vehicle drive shaft are connected through a mechanical transmission designed and realized by GKN. The device integrates a high efficiency single speed reduction unit with the differential. It is cooled with the lubricant oil and can host inside, for the hybrid applications, an electrically driven disconnect clutch to decouple the e-machine rotor shaft from the wheels at high speed. To safely manage the vehicle parking condition for BEV applications, a park lock system based on a 12 V DC e-motor can be added. In future, it is expected that this system can be avoided, instead managing the vehicle parking condition through a functional integration with the EBP (Electric Parking Brake) directly acting on the wheels brake units. As introduced in section 2, in FITGEN two reduction ratios, i.e. 1:9.6 and 1:12.5, are considered. In parallel, it will be investigated, at calculation level, the feasibility of a deeper integration of the axle electric drive with the transmission. The idea consists in using the transmission cooling-lubricating oil also to cool the e-drive (e-machine and inverter), with the help, if necessary, of a 12 V electrohydraulic cooling-lubricating pump and a heat exchanger. This configuration is designed to avoid the connection to the vehicle water cooling circuit (particularly not desired for rear e-axle solutions) and in this way limiting the e-axle vs. vehicle interfaces to the mechanical (drive shafts) plus the electric power (DC) and signal ones.

3.3. Design guidelines for the SiC-inverter

FITGEN aims at functionally integrating BPM-SM with the SiC-inverter and DC/DC converter and on-board charger according to the schematic presented in Figure 1. Here, the main preliminary design considerations for the power electronic components are presented.

3.3.1. VA size of the m-phase inverter with or without the DC/DC converter

The inverter size is defined as the sum of the Safe Operating Area (SOA) Volt-Ampere (VA) rating of the m phases of the converter. Three-phase and six-phase scenarios are considered, with the voltage and current size of the power modules related to the size of the e-motor. Given the peak power of the motor P_{max}, the absorbed electric power (AC-side) is:

$$P_{e,max} = \frac{m}{2} \cdot \left(\hat{V}_{ph}\hat{I}_{ph}cos\varphi\right)_{wc} = \frac{m}{2} \cdot \hat{V}_{ph,max}\hat{I}_{ph,max}cos\varphi_{wc} \quad (15)$$

Considering the motor efficiency, the motor power emerges as $P = P_e/\eta$:

$$P_{max} = \frac{m}{2} \cdot \hat{V}_{ph,max}\hat{I}_{ph,max}(\eta\ cos\varphi)_{wc} \quad (16)$$

The VA_{SOA} term can be put in evidence in (*(17)*).

$$VA_{motor} = \frac{m}{2} \cdot \hat{V}_{ph,max}\hat{I}_{ph,max} = \frac{P_{max}}{(\eta\ cos\varphi)_{wc}} \quad (17)$$

This defines the VA requirement for this motor, given the motor peak power P_{max} and performance figures $(\eta\ cos\varphi)_{wc}$. The first SOA sizing coefficient follows:

$$k_{motor,SOA} = \frac{VA_{motor}}{P_{max}} = \frac{1}{(\eta\ cos\varphi)_{wc}} \quad (18)$$

Considering that each inverter phase (half-bridge module) has a voltage rating equal to V_{SOA} and a continuous current rating of I_{SOA}, if sinusoidal waveforms are considered, it turns out that $V_{SOA} \geq \sqrt{3} \cdot \hat{V}_{ph,max}$ and $I_{SOA} \geq \hat{I}_{ph,max}$. Two other coefficients are introduced, to consider the SOA margin with respect to the motor peak requirements:

$$k_{V,SOA} = \frac{V_{SOA}}{\sqrt{3} \cdot \hat{V}_{ph,max}} \quad (19)$$

$$k_{A,SOA} = \frac{I_{SOA}}{\hat{I}_{ph,max}} \quad (20)$$

Finally, the inverter size is:

$$VA_{SOA} = k_{V,SOA}\ k_{A,SOA}\ VA_{motor} = \left(k_{V,SOA}\ k_{A,SOA}\ k_{motor,SOA}\right) \cdot\ P_{max} \quad (21)$$

Here, the adoption of the DC/DC converter does reduce the voltage factor $k_{V,SOA}$ with respect to direct battery connection. For example, for a battery voltage spanning from 320 V (full discharge) to 420 V (full charge), the factor $k_{V,SOA}$ is 31% larger than for the case with the DC/DC regulating the dc-link. This conclusion is independent from the number of phases. Conversely, the adoption of the 6-phase configuration slightly improves the e-motor efficiency for the same inverter size, and this reflects into the motor merit factor $k_{motor,SOA}$.

3.3.2. DC-link capacitor current size

One key aspect when comparing 3-phase and 6-phase DC/AC converters is the size of the DC-link capacitor. The key figure of comparison in this section is the rms current value of the DC-link capacitor current, as produced by the m-phase inverter in the respective worst-case design points. It must be noted that the worst-case design condition for the capacitor does not coincide with the one considered for the inverter VA size. According to (Kolar & Round, 2006), the rms current in the DC-link capacitor of a three-phase inverter is:

$$I_{C,rms} = I_{ph,rms} \cdot \sqrt{2M\left[\frac{\sqrt{3}}{4\pi} + (cos\phi)^2\left(\frac{\sqrt{3}}{\pi} - \frac{9}{16}M\right)\right]} \quad (22)$$

Where M is the modulation index of the inverter, $I_{ph,rms}$ is the rms motor phase current and $\cos\phi$ is the motor power factor M is defined as the amplitude of the output phase voltage normalized by half the dc-link voltage $M = \hat{V}_{ph}/(V_{dc}/2)$. Its range is from 0 to $\frac{2}{\sqrt{3}} = 1.155$. According to (Bojoi, et al., 2002), the formula valid for the six-phase inverter is:

$$I_{C,rms} = I_{ph,rms} \cdot \sqrt{2M[0.243 + (cos\phi)^2(2.468 - 2.25M)]} \quad (23)$$

It must be remarked that the $I_{ph,rms}$ in ((23)) is exactly half the one in ((22)), due to the different number of phases. The comparison is summarized in the charts of Figure 6, where the factor two is account for. The results show a slight advantage of the 6-phase solution for high values of power factor (the two curves for $cos\phi = 1$ are similar) and a more substantial advantage for realistic values of power factor (for $cos\phi = 0.8$, the rms current is 10% lower with 6 phases). For now, the analysis is limited to the case of a single PWM carrier for the 6-phase case. Further minimization of $I_{C,rms}$ can be obtained by using two shifted PWM carriers.

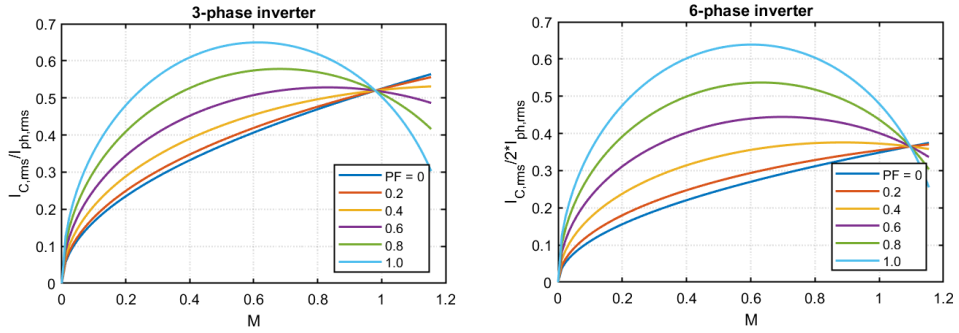

Figure 6: Rms current absorbed by the DC-link capacitor. A) produced by a 3-phase inverter, b) or by 6-phase inverter. Note: the capacitor current is normalized by the phase current of the reference 3-phase motor ($2I_{ph,rms}$ for the 6-phase case).

3.3.3. Inverter control strategy

The development of efficient and reliable control strategies is of great importance to control the torque generation of the BPM-SM in the whole vehicle operational range. The high non-linearities caused by the magnetic saturation effect (Meessen, Thelin, Soulard, & Lomonova, 2008) together with electrical parameter variations due to machine ageing, manufacture tolerances and temperature dependency confirm the importance of relying on a robust control strategy that ensures the correct operation of the drive during its whole lifecycle. The most common synchronous machine torque control approaches consist of regulating the machine stator currents in the synchronous dq reference frame (Kim & Sul, 2007). Although PI (Proportional Integral) based FOC (Field Oriented Control) control is one of the most matured control approaches, non-linear control strategies such as the SMC (Sliding Mode Control) based FOC are also considered as appropriate because of their robustness against parameter variations. These strategies must be complemented with an optimal current set-point generation algorithm (Jung, Hong, & Nam, 2013) to drive propulsion system through the maximum efficiency points, including Field Weakening (FW) and deep FW operation when required. In FITGEN, both PI based FOC strategy and second order SMC will be assessed and compared in terms of e-axle efficiency, performance and execution time consumption. The most suitable control approach will be implemented in the SiC inverter control module. Additionally, the optimal current references will be calculated for the whole torque and speed operation regions, minimizing the copper losses at low speeds and the magnetic losses at high speeds.

3.4. Integration of the fast charging via DC/DC converter and integrated on-board charger

The FITGEN e-axle makes use of an efficient DC/DC-conversion stage, with smart control features enabling the rotor-synchronised DC-link, and the flexible handling of the number of phases of the motor between six and three, depending on the operating conditions of the vehicle. The high voltage DC/DC-converter steps-up the battery voltage from a nominal 320-420 V, creating a controlled DC-link with a maximum rating up to 750 V. Besides the just described motor and inverter current rating reduction (450 to 200 A rms if 3-phase, 225 to 100 A rms if 6-phase). This offers several advantages, described in the section below.

3.4.1. DC fast charge and smart DC-link control

The key features enabled by the DC/DC converter are (i) compatibility with high voltage DC-chargers up to 750 V (with flexibility to lower rated values) and (ii) smart-use of the DC-link voltage.

With respect to fast DC-charging, the FITGEN architecture will be compatible with current and next generation high voltage DC chargers, adaptable with flexibility to chargers with nominal value up to 800 V DC. Dealing with the Smart DC-link control through the DC/DC unit, the highly dynamic response of the DC-link voltage enables instantaneous optimisation of the voltage level in traction. This brings the following benefits: (i) the minimisation of the DC-link voltage according to the vehicle speed in the low and medium speed ranges, which minimises the inverter switching loss, and (ii) the rotor-synchronised DC-link strategy, i.e. the dynamic synchronisation of the DC-link voltage to the motor phase angle. This is further useful in the low speed range of the vehicle, to reduce the inverter switching loss by avoiding the commutation of selected inverter legs. In rotor-synch DC-link mode the DC-link voltage will be regulated to vary at 6-times the fundamental frequency of the motor and only 2 of the 6 inverter legs per time will switch, whereas the duty cycles of the remaining 4 inverter phases are clamped to continuous low or continuous high states.

3.4.2. On-board integrated charger

Beyond the DC fast charging capability in the full range 400-to-800 V, a low-to-mid power AC/DC on-board charger as much integrated as possible into the powertrain is also foreseen to be investigated. Three options are considered: (i) single-phase charging with EMI filter, (ii) single-phase charging with EMI filter and PFC (power factor corrector) and (iii) 3-phase charging with EMI filter. The second option uses the inverter switches and the e-machine stator phases as coupled inductances to realize an interleaved PFC rectifier. This layout is preferable, because it maintains the advantages of integrated chargers and, at the same time, it minimizes the negative impact on the grid waveform quality, cf. the Renault Chameleon thanks to the PFC stage. However, its limitations are the lack of electrical insulation and the non-compatibility with the requirements of three-phase supply with PFC.

4. Conclusions

This paper presents the interim results of the H2020 project FITGEN. The project aims at developing and delivering a functionally integrated e-axle ready for implementation in third generation electric vehicles, demonstrated on a A-segment BEV platform. Preliminary results show that, to match the e-motor power density target, the rotational speed of 20,000 – 22,000 rpm is needed, calling for coupling the motor with a single speed transmission at a reduction ration of 1:12.5. FLW against HPW are preferred for the motor stator design, with the group inverter-motor-transmission mounted in rear-wheel driving configuration. Concerning power electronics, a 6-phase SiC-inverter is selected to increase energy efficiency, combined with a DC/DC and smart DC-link to enable fast charge and optimise voltage level in traction. The system is complemented with an on-board charger, preliminarily selected in single-phase charging with EMI filter configuration.

Acknowledgements

The authors are grateful to the European Commission for the support to the present work, performed within the EU H2020 project FITGEN (Grant Agreement 824335) and to Dr. Dragan Simic for the rendering of Figure 1.

References

Bojoi, R., Caponet, M. C., Grieco, G., Lazzari, M., Tenconi, A., & Profumo, F. (2002). Computation and measurements of the DC link current in six-phase voltage source PWM inverters for AC motor drives. *Proceedings of the Power Conversion Conference* . Osaka: IEEE.

Boldea, I., & Nasar, S. (2010). *The induction machine handbook.* CRC press.

Borisavljevic, A. (2013). *Limits, Modeling and Design of High-Speed Permanent Magnet Machines.* Springer-Verlag.

Boston Consulting . (2018). *The future of Battery Production for Electric Vehicles.*

EU Commission CORDIS. (2019). *Functionally Integrated E-axle Ready for Mass Market Third GENeration Electric Vehicles*. Retrieved from https://cordis.europa.eu/project/rcn/218519/factsheet/en

EU Commission, S. E. (2016). *Integrated SET-Plan Action 7 - Become competitive in the global battery sector to drive e-mobility and stationary storage forward.*

IEA. (2018). *Global EV Outlook 2018.*

Insideevs.com. (2018). *September 2018 Plug-In Electric Vehicle Sales Report Card*. Tratto da https://insideevs.com/news/339986/september-2018-plug-in-electric-vehicle-sales-report-card/

Jung, S., Hong, J., & Nam, K. (2013). Current minimizing torque control of the IPMSM using Ferrari's method. *IEEE Transactions on Power Electronics*, 5603–5617.

Kim, Y., & Sul, S. (2007). Torque control strategy of an IPMSM considering the flux variation of the permanent magnet. *Industry Applications Society Conference (IAS).*

Kolar, J. W., & Round, S. D. (2006, July). Analytical calculation of the RMS current stress on the DC-link capacitor of voltage-PWM converter systems. *IEE Proceedings - Electric Power Applications, 153*(4), 535-543. doi:10.1049/ip-epa:20050458

Meessen, K., Thelin, P., Soulard, J., & Lomonova, E. (2008). Inductance calculations of permanent-magnet synchronous machines including flux change and self- and cross-saturations. *IEEE Transactions on Magnetics, 44*(10), 2324-2331.

Mühlethaler, J., Biela, J., & Kolar, J. W. (2012). Core Losses Under the DC Bias Condition Based on Steinmetz Parameters. *IEEE Transaction on Power Electronics*.

Sullivan, C., & Zhang, R. (2014). Simplified Design Method for Litz Wire. *IEEE Advanced Power Electronics Conference.*